Structure of PITPβ in Complex with Phosphatidylcholine: Comparison of Structure and Lipid Transfer to Other PITP Isoforms[†,‡]

Paul B. Vordtriede,[§] Chuong N. Doan,[§] Jacqueline M. Tremblay,[||,⊥] George M. Helmkamp, Jr.,[||] and Marilyn D. Yoder*[,§]

Division of Cell Biology and Biophysics, University of Missouri−Kansas City, Kansas City, Missouri 64110-2499, and Department of Biochemistry and Molecular Biology, University of Kansas Medical Center, Kansas City, Kansas 66160-7421

Received June 21, 2005; Revised Manuscript Received August 15, 2005

ABSTRACT: Phosphatidylinositol transfer protein (PITP) is a ubiquitous eukaryotic protein that preferentially binds either phosphatidylinositol or phosphatidylcholine and catalyzes the exchange of these lipids between membranes. Mammalian cytosolic PITPs include the ubiquitously expressed PITPα and PITPβ isoforms (269−270 residues). The crystal structure of rat PITPβ complexed to dioleoylphosphatidylcholine was determined to 2.18 Å resolution with molecular replacement using rat PITPα (77% sequence identify) as the phasing model. A structure comparison of the α and β isoforms reveals minimal differences in protein conformation, differences in acyl conformation in the two isoforms, and remarkable conservation of solvent structure around the bound lipid. A comparison of transfer activity by human and rat PITPs, using small unilamellar vesicles with carefully controlled phospholipid composition, indicates that the β isoforms have minimal differences in transfer preference between PtdIns and PtdCho when donor vesicles contain predominantly PtdCho. When PtdCho and PtdIns are present in equivalent concentrations in donor vesicles, PtdIns transfer occurs at approximately 3-fold the rate of PtdCho. The rat PITPβ isoform clearly has the most diminished transfer rate of the four proteins studied. With the two rat isoforms, site-directed mutations of two locations within the lipid binding cavity that possess differing biochemical properties were characterized: I84α/F83β and F225α/L224β. The 225/224 locus is more critical in determining substrate specificity. Following the mutation of this locus to the other amino acid, the PtdCho transfer specific activity became PITPα (F225L) $\approx$ PITPβ and PITPβ (L224F) $\approx$ PITPα. The 225α/224β locus plays a modest role in the specificity of both isoforms toward Cer*P*Cho.

Phosphatidylinositol transfer proteins (PITP)[1] are eukaryotic proteins with the ability to bind and transfer either phosphatidylinositol (PtdIns) or phosphatidylcholine (PtdCho) between intracellular membranes (*1*−*3*). They have been implicated in numerous signal transduction and vesicular trafficking pathways (*4*−*7*). Two isoforms, PITPα and PITPβ, are expressed in all studied mammalian species (*2*, *8*) and sequence homologues detected in all known metazoans. Phospholipid transfer in eukaryotic cells is also mediated by Sec14p (a yeast PITP) and phosphatidylcholine transfer protein (PCTP). Crystal structures of the α isoform of rat (*9*), mouse (*10*), and human (*11*) have been reported, as well as yeast Sec14p (*12*) and human PCTP (*13*). Although rat PITPα is a functional homologue to Sec14p in yeast, the two proteins do not share common folds. Unlike Sec14p, the phospholipid binding site in PITPα is completely buried in the interior of the protein. PITPα shares a similar fold to the steroidogenic acute regulatory protein-related lipid transfer (START) domain first observed in human MLN64 (*9*, *14*). PCTP is classified as a START domain protein based on both primary and tertiary structure conservation.

PCTP and PITP exhibit significantly different conformations of their bound phospholipid. The bound PtdCho in PCTP has a C-shaped conformation of the acyl chains (*13*), whereas the acyl chains in PITPα are more extended. In the structure of mouse PITPα in the absence of phospholipid (*3*, *10*) there are two molecules in the asymmetric unit, forming a dimer. In addition, the loop containing helix B has a different conformation from the holo form of PITPα. This loop has been termed the lipid exchange loop, with the open structure a putative membrane-associated form and the closed form being the lipid-loaded, cytoplasmic form.

PITPα is primarily found in the cytosol and nucleus, while PITPβ is found associated with the Golgi complex (*15*, *16*). Localization of PITPβ to the Golgi complex requires the protein kinase C-dependent phosphorylation of Ser262; yet phosphorylation had no effect on phospholipid transfer activities (*17*). This Ser residue is conserved in all known

[†] Supported by National Institutes of Health Grant GM59162.

[‡] Atomic coordinates and structure factors have been deposited at the Protein Data Bank, accession code 2A1L.

* Corresponding author. Phone: 816-235-1986. Fax: 816-235-1503. E-mail: YoderM@umkc.edu.

[§] University of Missouri−Kansas City.

[||] University of Kansas Medical Center.

[⊥] Current address: Department of Biomedical Sciences, Tufts University Cummings School of Veterinary Medicine, North Grafton, MA 01536-1895.

[1] Abbreviations: Cer*P*Cho, sphingomyelin; ER, endoplasmic reticulum; LacPtdEtn, *N*-lactosyl-1,2-dioleoylphosphatidylethanolamine; PCTP, phosphatidylcholine transfer protein; PITP, phosphatidylinositol transfer protein; PtdCho, phosphatidylcholine; PtdEtn, phosphatidylethanolamine; PtdIns, phosphatidylinositol; PtdOH, phosphatidic acid; rmsd, root mean square deviation; START, steroidogenic acute regulatory protein-related lipid transfer.

10.1021/bi051191r CCC: $30.25
Published on Web 10/20/2005

mammalian PITPβ proteins but is a proline residue in mammalian PITPα sequences. Overexpression of PITPα in NIH3T3 cells, but not PITPβ, activates phospholipase A_2 and shortens the G_1 phase of the cell cycle (*18*). In contrast, overexpression of PITPβ results in decreased growth rate and exhibits effects indicating an involvement in maintaining Cer*P*Cho steady-state levels (*19*). It has been proposed that PITPβ may be involved in diacylglycerol production (*20*).

In mice, a mutation in the PITPα gene results in the *vibrator* phenotype which causes a 5-fold reduction in protein levels and results in progressive action tremors, degeneration of brain stem and spinal cord neurons, and juvenile death. Interestingly, PITPβ does not compensate for the loss of PITPα (*21*). Using PITPα- and PITPβ-deficient embryonic stem cells from mice, Alb et al. (*22*) conclude that PITPβ has an essential housekeeping role where deficiency is lethal early in embryonic development. In contrast, PITPα-deficient embryonic stem cells are compromised neither in growth nor in bulk phospholipid metabolism. PITPα is, however, required for neonatal survival. An unexpected role for PITPα was suggested in regulating phospholipid transport in the endoplasmic reticulum (ER), endocrine pancreas function, and glycogen metabolism due to numerous compromised lipid absorption and homeostatic problems and severe hypoglycemia. These observations suggest roles for PITPα in signaling pathways that interface trafficking of lipid cargo from the ER and glucose homeostasis in mammals (*22*).

Using site-directed mutagenesis of human PITPα and monitoring both the occupancy of the lipid binding cavity and the intermembrane lipid transfer, Tilley et al. (*11*) identified two residues that were indispensable for the interaction of PtdIns with the protein. Mutants K61A and N90F/L lost virtually all activity toward PtdIns but retained full activity toward PtdCho. Indeed, these amino acids most likely participate in noncovalent interactions with the inositol ring system but do not contact the choline quaternary ammonium moiety. While the above-mentioned analyses of phospholipid specificity for human or rat PITPα have provided important information on critical residues within the lipid binding cavity, particularly those residues that make contact through their van der Waals radii with the polar headgroup, they do not address substrate differences between the two predominant PITP isoforms expressed in higher eukaryotic cells.

The current investigation was undertaken to determine structural differences between PITPα and PITPβ and to elucidate the effects of mutations affecting amino acid residues proposed to play a role in differential isoform phospholipid transfer capabilities. The structural studies revealed very subtle differences in protein conformation, differences in acyl conformation in the two isoforms, and remarkable conservation of solvent structure around the bound lipid. Site-directed mutations of two locations manifesting amino acids of differing biochemical properties provide insight into differences in phospholipid transfer rates between the isoforms.

EXPERIMENTAL PROCEDURES

Reagents. Chicken egg yolk PtdCho, bovine liver phosphatidylethanolamine (PtdEtn), 1,2-dioleoylphosphatidic acid (PtdOH), bovine liver PtdIns, *N*-lactosyl-1,2-dioleoyl-PtdEtn (LacPtdEtn), porcine brain Cer*P*Cho, and cholesterol were purchased from Avanti Polar Lipids (Alabaster, AL). Cholesteryl oleate was obtained from Sigma (St. Louis, MO). All lipids were >95% pure on analysis by thin-layer chromatography. Radiolabeled lipids acquired from commercial sources included bovine brain [*N-methyl*-^{14}C-*choline*]-Cer*P*Cho (2.1 Gbq·mmol^{-1}), Amersham Biosciences (Piscataway, NJ), and [9,10-^{3}H]oleic acid (310 Gbq·mmol^{-1}), [1-^{14}C-*oleoyl*]-1-palmitoyl-2-oleoyl-PtdCho (1.9 Gbq·mmol^{-1}), [2-^{3}H-*inositol*]PtdIns (407 Gbq·mmol^{-1}), and [1-^{14}C-*oleoyl*]-cholesteryl oleate (2.1 Gbq·mmol^{-1}), NEN Life Sciences (Boston, MA). Cholesteryl [9,10-^{3}H]oleate was synthesized according to published procedures (*28*). Poly(ethylene glycol) 400 was purchased from Sigma, and Paratone was manufactured by Exxon Chemicals.

Full-length cDNAs encoding rat and human PITPα were prepared in our laboratory (*8*, *23*); those encoding rat and human PITPβ were generously donated by K. Hosaka (Maebashi, Japan). Restriction endonucleases were supplied by Promega (Madison, WI), New England Biolabs (Beverly, MA), or Fisher BioReagents (Fair Lawn, NJ). T4 ligase and *Taq* DNA polymerase were products of Promega or Fisher; Geneclean was obtained from Bio101 (Vista, CA). Oligonucleotides were synthesized commercially (Integrated DNA Technologies, Coralville, IA; MWG Biotech, Charlotte, NC). Bidirectional DNA sequence analyses were carried out by the University of Kansas Medical Center Biotechnology Support Facility. The galactose-specific agglutinin, RCA-120, was purified from locally available castor beans to electrophoretic homogeneity according to a published protocol (*24*). Other chemicals were of reagent grade and of the highest purity available.

Expression and Purification of Recombinant Proteins. Methods to express and purify PITPs from cell-free lysates of *Escherichia coli* and to determine their concentration have been reported (*25*−*27*). By the criteria of protein staining of electrophoretically resolved polyacrylamide gels and immunologic detection of nitrocellulose blots, all proteins appeared homogeneous and intact. Rabbit IgG fractions were generated to Q^{260}KDPVKGMTADD^{271} of rat PITPα and Q^{251}KELETMRKKGSVR^{264} of rat PITPβ. Proteins were assayed with their endogenously bound phospholipids, typically phosphatidylglycerols of bacterial origin.

Oligonucleotide-Directed Mutagenesis. Because the human PITPα and PITPβ cDNAs were in pBluescript and pCMV5 plasmids, respectively, primers were constructed to permit their PCR amplification as well as introduce an *Nde*I site at the 5′-terminus of the open reading frame and a *Bam*HI site 13 bp downstream of the 3′-terminus. The coding regions were excised, purified using Geneclean, and ligated into the pET-11c vector (Novagen, Madison, WI). Site-directed mutagenesis was carried using the QuikChange (Stratagene, La Jolla, CA) polymerase chain reaction protocol and reagents. Pairs of complementary primers (27−30 bases in length) were designed to introduce the following mutations, singly or doubly: I84F and F225L into wild-type rat PITPα and F83I and L224F into wild-type rat PITPβ. Following transformation into *E. coli* strain XL1-Blue (Stratagene), plasmid DNA was purified (Qiagen, Valencia, CA) and characterized spectroscopically and structurally. Comparison of results obtained from sequencing of the open reading

frames in both directions confirmed that the desired mutants had been engineered.

Intermembrane Lipid Transfer Activity. Lipid transfer activity of PITPs was determined by measuring the rate of radiolabeled phospholipid from donor to acceptor vesicles, as described (*28*). Small unilamellar vesicles were prepared by rapid injection of ethanol/dimethyl sulfoxide (80:20 vol %) solutions, followed by brief exposure to bath sonication. Prior to use, vesicles were passed through a polyvinylidene fluoride filter (0.45 μm pore; Millex, Millipore, Fisher Scientific, Pittsburgh, PA). Bulk membrane lipids were either egg yolk PtdCho or liver PtdEtn; a small amount of anionic phospholipid (PtdOH or PtdIns) was present in quantities as indicated in Tables 6 and 7. Transferable substrates in donor vesicles included radiolabeled PtdIns, PtdCho, or Cer*P*Cho. Donor vesicles always contained 10 mol % LacPtdEtn to provide interaction with the RCA-120 agglutinin. Acceptor vesicles were prepared with a trace amount ($\leq$0.5 mol %) of either cholesteryl [^{3}H]oleate or cholesteryl [^{14}C]oleate as an internal standard in the double-isotope analysis of vesicle recovery and extent of phospholipid transfer. Vesicle concentration was based upon lipid phosphorus determination following chloroform/methanol (50:50 vol %) extraction of suitable aliquots. The buffer employed in vesicle preparation and transfer assays was 10 mM HEPES-Na, 50 mM NaCl, and 1 mM Na_2EDTA (pH 7.4); in some cases the NaCl concentration was varied. Assays were performed at 37 °C for 30 min; controls were carried out in the absence of PITP. Separation of vesicle populations was achieved by agglutination and precipitation of LacPtdEtn-containing donor membranes in the presence of RCA-120 agglutinin (*28*). Acceptor vesicle recovery was 85−95%; contamination by donor vesicles was <10%. Care was taken to ensure that assays were performed under conditions in which the rate of transfer was directly proportional to the amount of transfer protein added.

Crystallization. Purified rat PITPβ was prepared, and the phospholipids were exchanged for dioleoyl-PtdCho following similar procedures for the preparation of rat PITPα-PtdCho (*29*). The protein was crystallized by vapor diffusion in 6 μL hanging drops (5 μL of protein at 11.64 mg/mL plus 1 μL of reservoir solution) equilibrated against 1 mL of reservoir solution [40% w/v poly(ethylene glycol) 400, 0.1 M NaCl, 0.1 M sodium−potassium phosphate buffer, pH 6.2] in 24-well VDX plates (Hampton Research). Bipyramidal-shaped crystals grew to maximum dimensions of 0.4 × 0.3 × 0.2 mm in 2 weeks. Crystals were cryoprotected by passage through paratone and frozen by rapid submersion in liquid nitrogen. Crystal and X-ray data collection information is summarized in Table 1.

Data Collection and Structure Determination. X-ray data were collected on a cryocooled crystal at beamline 22-ID at the Advanced Photon Source (Chicago, IL) using a MAR220 CCD detector. The crystal to detector distance was 225 mm. The oscillation range was 1° per frame with an exposure time of 5 s per frame. Diffraction images were indexed and scaled with HKL2000 (*30*). The three-dimensional structure was determined by molecular replacement using the AMoRe package implemented in CCP4i (*31*) using portions of PDB code 1T27 as the search model. During the course of this study, the PtdCho molecule of PITPα-PtdCho of PDB code 1FVZ was corrected for improper stereochemistry, and the coordinates were resubmitted as 1T27. Missing portions of the model were manually built into electron density maps iteratively using the computer graphics program O (*32*) alternated with refinement cycles. Refinement was done with CNS v1.1 (*33*) using all of the diffraction data minus 10% reserved for R_{free} validation (*34*). One PtdCho and the solvent molecules were added after all observed amino acid residues were modeled. Water peaks were assigned from $F_o - F_c$ electron density maps using the default protocol as implemented in CNS and manually verified in O. The final refined model consists of protein residues 2−185, 187−270, one molecule of dioleoyl-PtdCho, and 157 water molecules. No residues are in disallowed regions of a Ramachandran plot as defined by PROCHECK (*35*). The coordinates and structure factors are deposited in the PDB, accession code 2AIl.

Table 1: Crystal Parameters and X-ray Data Collection Statistics

Crystal Parameters	
cell dimensions *a*, *b*, *c* (Å)	65.948, 65.948, 133.513
unit cell volume (Å^3)	5.8×10^5
V_M (Å^3 Da^{-1})	2.31
molecules per asymmetric unit	1
estimated solvent content (%)	46.3
diffraction limit (Å)	2.0
Data Collection Statistics	
wavelength (Å)	1.0000
temperature (K)	100
spacegroup	$P4_32_12$
resolution range (Å)	50.0−2.18 (2.18−2.26)[a]
no. of observations	312298
no. of unique reflections	15998 (1281)
multiplicity	19.5 (6.5)
completeness overall (%)	97.4 (80.6)
R_{sym} overall (%)[b]	8.3 (27.5)

[a] Numbers in parentheses relate to the highest resolution shell. [b] $R_{sym} = \sum(|I - \langle I\rangle|)/\sum I$.

Generation of Electrostatic Surfaces and Lipid Cavity. Electrostatic charge distribution was calculated by GRASP (*36*). Regions of negative and positive potential were colored to an approximate range of −25 (red) and +25 (blue) k_BT, where k_B is the Boltzman constant and T is temperature. Molecular and electrostatic surface files were exported from GRASP, displayed in DeepView (*37*), and rendered using POVRAY (www.povray.org). The lipid cavity depicted in Figure 4 was calculated by VOIDOO (*38*) using a probe radius of 1.0 Å, a grid spacing of 1.0 Å, and a van der Waals growth factor of 1.10 Å.

RESULTS

PITPβ-PtdCho Crystal Structure. The structure of the β isoform was determined by molecular replacement using the rat PITPα lipid binding core as a search model (PDB code 1T27; residues 16−33, 39−45, 58−117, and 193−251). There was little difficulty in tracing the remaining loop regions, the exception being Asp186 in a solvent-exposed regulatory loop region. This residue is presumed to be disordered and is not included in the model. The refinement statistics are summarized in Table 2.

The prominent structural features of PITP include a large concave β-sheet and several long helices (Figure 1). Strands 2 and 7 define the edges of the β-sheet. The three functional regions first identified in PITPα-PtdCho are present in the

Table 2: Refinement Summary

resolution range (Å)	38.23−2.18
R-factor(%)	20.2
R_{free} (%)	25.1
protein atoms[a]	2199
ligand atoms	54
water molecules	156
rmsd bond lengths (Å)[b]	0.006
rmsd bond angles (deg)[b]	1.2
B-factor (Å^2)	
average	60.1
main chain	57.61
side chains	59.62
lipid atoms	69.05
water molecules	65.03

[a] Non-hydrogen protein atoms inserted into the model. [b] Root mean square deviation from ideal values.

β isoform. The lipid binding core is composed of strands 1−6 and 8 and helices A and F. The regulatory loop begins at the C-terminus of strand 6 and ends at the N-terminus of strand 8. The C-terminal region begins with helix G. Helix B is a putative lipid exchange loop proposed by Schouten et al. (*10*) and is present in a closed conformation in rat PITPβ-PtdCho, as expected for the phospholipid-loaded form of the protein.

Comparison of PITPα *and PITP*β *Structures.* The structure of rat PITPβ-PtdCho is very similar to rat PITPα-PtdCho (*9*), a predictable outcome because the two polypeptides share 77% sequence identity. The two rat PITP isoform structures have an C^{α} root mean square deviation (rsmd) of 0.785 Å^2 between all residues from 2 to 270. The primary differences are in the last six residues of the C-terminal loop. This extended coil in PITPβ reaches more toward the interior of the lipid binding core than in the PITPα-PtdCho structure. The human PITPα with bound phosphatidylinositol (PDB code 1UW5) is highly conserved to the rat PITPs at both the primary and tertiary levels (*11*). The rat and human PITPα structures are superimposable with a root mean square deviation (rmsd) of 0.914 Å^2 while the human PITPα structure has a rmsd of 0.934 Å^2 with respect to rat PITPβ (Figure 1B).

Differences in Ligand Structure between PITPα *and PITP*β. The phospholipid ligand in both of the rat PITP isoform structures is chemically identical, dioleoyl-PtdCho. The orientation of the choline headgroup, the glycerol backbone, and the phosphate group is similar in the two structures, with a rmsd of 1.38 Å^2 between all nonacyl chain atoms. The torsion angles between atoms of the headgroup ($\alpha_1-\alpha_6$) and glycerol backbone ($\theta_1-\theta_4$) in the rat PITPs and the human PITPα-PtdIns structures are tabulated in Table 3. This set of torsion angles is very similar in the rat structures; the most notable exceptions are torsion angles α_5 and α_6 of the PtdCho-complexed structures, which describe the torsion angles of the ethylene group between the phosphorus and nitrogen of the choline headgroup. The electron density in this area in both rat PITPα and rat PITPβ, although clear, is tubular shaped and lacks a clear definition of carbon orientations. The observed differences in these torsion angles may reflect some flexibility of these atoms within the binding site.

Differences in the acyl chains of the same phospholipid in the two PITP isoforms as well as differences in the same isoform but different phospholipids are observed (Figure 2). The human PITPα-PtdIns structure has a bound PtdIns that likely has heterogeneous acyl chain composition, and therefore acyl carbons beyond carbon 9 in the *sn*-1 and *sn*-2 chains are not visible. The *sn*-1 and *sn*-2 acyl chains of PITPα-bound PtdIns lay in the opposite acyl channels from what is observed in the two PtdCho-bound structures. This is due to an approximate 180° rotation about the glycerol carbon 1 and carbon 2 bond, θ_3/θ_4.

When PtdCho is bound to each of the two rat PITP isoforms, subtle differences in orientation of the acyl chains are observed. In both isoforms, the *sn*-1 acyl chain is more extended than the *sn*-2 chain and roughly follows the same course within the lipid binding cavity. PITPα and PITPβ *sn*-1 chains have a rmsd of 2.67 Å^2 when comparing all acyl chain atoms. An exception to the near identical superposition of the *sn*-1 chain is a bulge caused by the side chain at Ile84 in PITPα and the corresponding position Phe83 in PITPβ (Figure 3). These residues have different rotamer conformations about χ_1. In PITPα Ile84 has a +sc (+gauche) conformation while in PITPβ the Phe83 rotamer is in a −sc (−gauche) conformation. Both side chains are in preferred

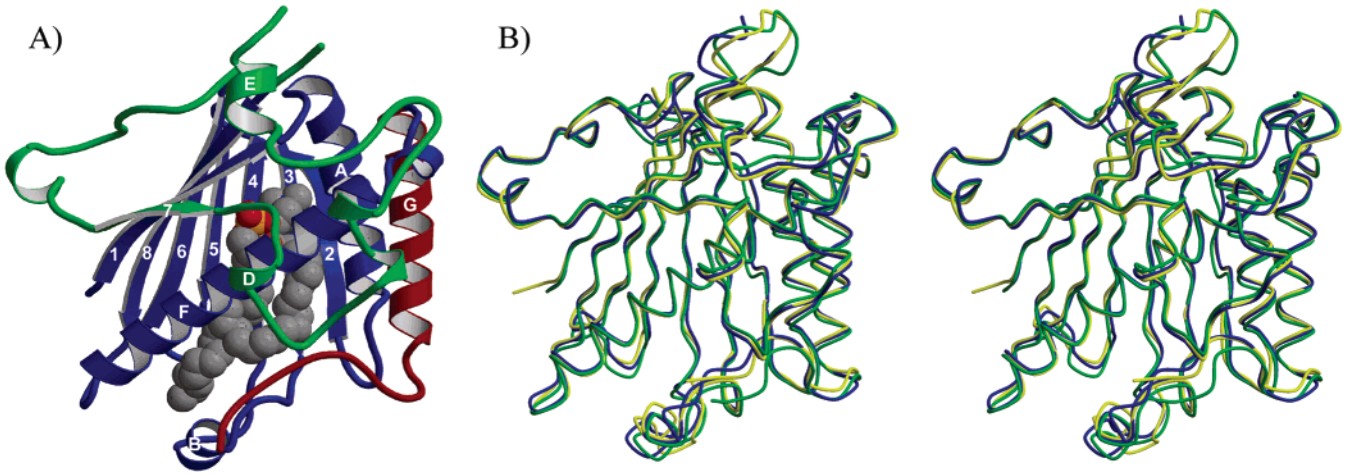

FIGURE 1: Ribbons and superposition of PITP structures. (A) Ribbon diagram of rat PITPβ-PtdCho. (B) Stereo image of the superposition of rat and human PITPs. The green trace depicts rat PITPα, the gold trace is human PITPα, and the blue trace is of rat PITPβ. The phospholipids are not shown.

Table 3: Comparison of Phospholipid Torsion Angles

	angle and atom definition[a]	PITPα:PtdCho (deg)	notation[b]	PITPβ:PtdCho (deg)	notation	PITPα:PtdIns (deg)	notation
α_1	C2−C1−O3P−P	−96.131	−ac	−107.199	−ac	−167.355	−ac
α_2	C1−O3P−P−O4P	97.910	+ac	3.302	+sc	153.704	ap
α_3	O3P−P−O4P−C4	−61.482	−sc	−80.691	−sc	73.133	+sc
α_4	P−O4P−C4−C5	−88.907	−sc	−125.390	−ac	−71.543	−sc
α_5	O4P−C4−C5−N	84.265	+sc	−143.118	−ac	NA[c]	
α_6	C4−C5−N−C6	−61.817	−sc	179.628	ap	NA	
θ_1	O3P−C1−C2−C3	−52.505	−ac	−60.677	−ac	93.679	+ac
θ_2	O3P−C1−C2−O2	58.710	+sc	0.787	+sc	−147.818	−ac
θ_3	C1−C2−C3−O3	−172.123	ap	−179.998	ap	−69.343	−sc
θ_4	O2−C2−C3−O3	72.963	+sc	64.678	+sc	166.813	ap
β_1	C1−C2−O2−C31	91.976	+ac	96.355	+ac	−81.561	−sc
β_2	C2−O2−C31−C32	−162.778	ap	−153.240	ap	−101.785	−ac
β_3	O2−C31−C32−C33	−90.116	−ac	−149.935	−ac	−108.688	−ac
γ_1	C2−C3−O3−C11	100.581	+ac	103.964	+ac	−82.944	−sc
γ_2	C3−O3−C11−C12	171.443	ap	−179.606	ap	16.855	sp
γ_3	O3−C11−C12−C13	143.402	+ac	−179.377	ap	−139.630	−ac

[a] Atom names for angle definitions using rat PITP atom nomenclature in PDB files. Torsion angles are defined according to Marsh (*40*) and Hauser et al. (*46*). [b] Notation refers to conformation with sp, syn-periplanar (cis), sc, syn-clinal (gauche), ac, anti-clinal (eclipsed), and ap, anti-periplanar (trans). [c] NA = no applicable angle in inositol headgroup.

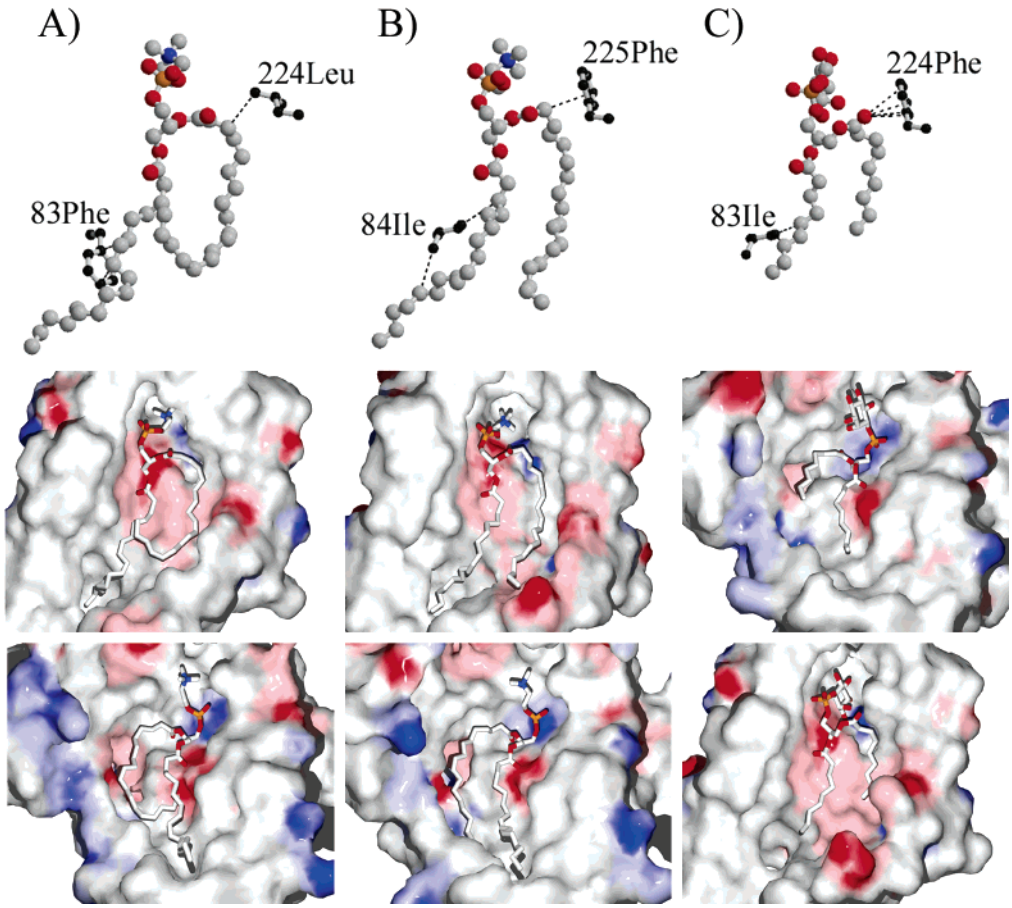

FIGURE 2: Phospholipid orientation in PITPs. Phospholipids are shown with standard CPK coloring. Top: Amino acids targeted for mutation during this study are highlighted. Dashed lines indicate interatomic distances ≤4.0 Å. Middle: Electrostatic surface representation of the lipid binding cavity with helix F and the regulatory loop removed for clarity. Bottom: Electrostatic surface rotated approximately 180° about a vertical axis relative to the middle orientation. β-strands 1−8 were removed for clarity. Key: (A) rat PITPβ with 1,2-dioleoyl-PtdCho (this study); (B) rat PITPα with 1,2-dioleoyl-PtdCho (PDB code 1T27); (C) human PITPα with bovine liver PtdIns (PDB code 1UW5).

rotamer conformations (*39*). This difference will be discussed below.

Most differences in lipid structure are seen in the *sn*-2 acyl chains of PtdCho. The last five carbons of the lipid bound to rat PITPβ and the last three carbons of the lipid bound to rat PITPα are oriented approximately 90° to each other when superimposed, with a rmsd of 3.09 Å^2 between all atoms in the *sn*-2 chain. This appears to be due to small differences in the lipid binding core and C-terminal loop. The conservative natural substitution of Ile40Val, comparing rat PITPβ and rat PITPα, results in the acyl chain in the α isoform bending slightly more toward the β-sheet of the lipid binding core. The acyl chain of the β isoform takes a more direct path down the lipid binding cavity. When the acyl

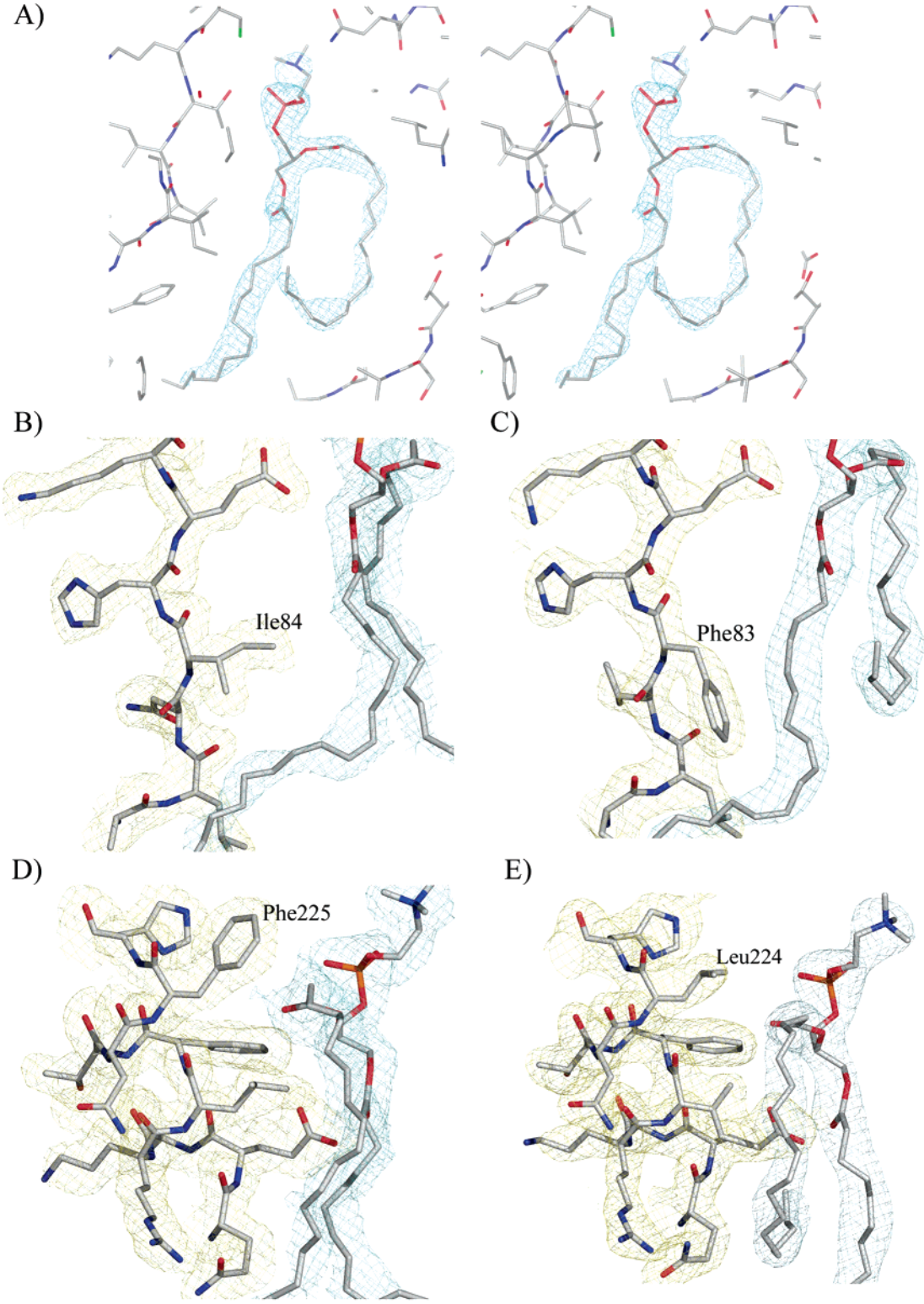

FIGURE 3: Electron density around residues of mutagenetic study. Electron density around protein atoms is shown in gold, while that around phospholipid atoms is in blue. Model atoms are colored by standard CPK coloring. (A) Stereo image of the $2F_o - F_c$ omit map calculated using model phases of the protein only and contoured around the phospholipid. With this view, the *sn*-1 acyl chain is on the left, and the *sn*-2 chain is on the right. (B) $2F_o - F_c$ electron density map around Ile84 of rat PITPα-PtdCho (PDB code 1T27). (C) $2F_o - F_c$ electron density map around Phe83 of rat PITPβ-PtdCho (this study). (D) $2F_o - F_c$ electron density map around Phe225 of rat PITPα-PtdCho. (E) $2F_o - F_c$ electron density map around Leu224 of rat PITPβ-PtdCho.

chains of *sn*-2 superimpose again, they are two carbons out of register, with the β isoform being two carbons longer. The sequence differences in the C-terminus of the two proteins also have an effect on the different *sn*-2 conformations. The side chain of Met267 in PITPα superimposes with the side chain of Thr266 in PITPβ. The side chains penetrate to approximately the same depth in both isoforms; therefore, the main chain of PITPα extends farther from the lipid binding core than in PITPβ to accommodate the longer Met side chain relative to Thr. The net effect is that in the β

Table 4: Torsion Angles of Acyl Chains of PITPs

	PITPβ-PtdCho				PITPα-PtdCho				PITPα-PtdIns			
angle[a] (*i*)	β_i[c]	notation[b]	γ_i[d]	notation	β_i	notation	γ_i	notation	β_i	notation	γ_i	notation
3	−149.935	−ac	−179.377	ap	−90.116	−ac	−143.402	−ac	−108.688	−ac	−139.630	−ac
4	147.395	+ac	107.101	+ac	93.181	+ac	−110.517	−ac	−154.656	ap	164.560	ap
5	−134.838	−ac	−119.634	−ac	152.418	ap	89.370	+sc	41.469	+ac	−63.394	−sc
6	89.007	+sc	−121.986	−ac	77.625	+sc	−174.092	ap	−147.585	−ac	−153.239	ap
7	−161.489	ap	152.587	ap	128.585	+ac	−124.715	−ac	172.588	ap	−175.744	ap
8	−177.944	ap	167.130	ap	−139.668	−ac	89.280	+sc	164.716	ap	−170.254	ap
9	97.160	+ac	80.228	+sc	−170.370	ap	157.183	ap	−143.575	−ac	−177.709	ap
10	124.124	+ac	140.078	+ac	161.392	ap	136.694	+ac				
11	0.030	sp	0.157	sp	−0.028	sp	0.128	sp				
12	116.927	+ac	129.257	+ac	−148.838	−ac	−140.027	−ac				
13	171.198	ap	−133.303	−ac	−169.798	ap	−115.579	−ac				
14	167.411	ap	82.236	+sc	102.728	+ac	−172.668	ap				
15	−119.631	−ac	121.444	+ac	−173.086	ap	−97.454	−ac				
16	84.162	+sc	117.250	+ac	−130.386	−ac	−156.223	ap				
17	−174.515	ap	179.845	ap	156.919	ap	104.749	+ac				
18	130.382	+ac	71.791	+sc	−121.535	−ac	133.310	+ac				

[a] Angle number, *i*, refers to the β_i or γ_i angle, numbered from the ester linkage. [b] Notation is as defined in Table 3. [c] β_i refers to torsion angles in the *sn*-2 chain. [d] γ_i refers to torsion angles in the *sn*-1 chain.

Table 5: Conserved Solvent Structure in Phospholipid-Bound PITPs[a]

rat PITPα-PtdCho (PDB code 1T27)	rat PITPβ-PtdCho (this study)	mouse PITPα (PDB code 1KCM)[b]
Wat2···(I112, T114)	Wat11···(I111, T113)	Wat16···(I112, T114, Wat35, C95)
Wat12···(Wat5, Q22)	Wat25···(Wat83, Q22)	Wat144
Wat127···Q22		Wat113···(Wat34, Y18, K195, H260)
Wat27···(Wat86, K61)	Wat49···(Wat66, K60)	Wat88···(Wat44, S39)
Wat7···(H116, K195, Y18)	Wat1···(H115, K194, Y18)	Wat34···(H116, K195, Y18, Wat113)
Wat15···(Y63, E86, K61)	Wat70···(Wat72, E85, K60)	
Wat8···(Wat114, T59, Q57, A88)	Wat7···(WatS94, T58, Q56, A87)	
Wat86···(Wat110, Wat27, L23, D248)	Wat66···(Wat90, Wat49, L23, D247)	Wat44···(Wat199, Wat88, Wat110, L23)
Wat110···(Wat86, Wat45)	Wat90···(Wat66, Wat73)	Wat199···Wat44
Wat5···(Wat12, Q22, N90)	Wat83···(Wat25, Q22, N89)	
Wat38···(Wat80, Q22, Q19)	Wat21···(Wat96, Q22, Q19, N89)	Wat7···(Wat32, Q22, Q19)
Wat80···(Wat38, Q19)	Wat96···(Wat21, Wat122, Q19, S60)	Wat191···(Wat32, Q19, N90, N90)
Wat45···(Wat110, S30, K61)	Wat73···(Wat90, S30, K60)	
Wat114···(Wat8, OP47, E46)	Wat94···(Wat7, Wat122, Wat117, N89)	
Wat4···(E86, T59, E86, T59)	Wat2···(E85, T58, E85, T58)	
Wat40···(A29, E33)	Wat32···(Wat62, A29, E33)	
Wat73···Q217		
Wat92···Q228	Wat62···(Wat32, Wat59, Q227)	
	Wat72···	
	Wat117···(Wat94, N45, E247, R244)	
	Wat122···(Wat94, Wat96, R244)	

[a] Waters are indicated as Wat followed by numbering as taken from the respective PDB coordinate files. Hydrogen bonding is indicated by horizontal dots, and bonding partners are indicated within parentheses with amino acids indicated in single letter code. The left indicated hydrogen bonding partner is structurally homologous across the row. [b] Only conserved waters are indicated for PITPα.

isoform the protein C-terminal residues lie closer to the main body of the structure and the *sn*-2 acyl chain bends inward. A comparison of torsion angles of the acyl chains in the three PITP structures is presented in Table 4. A cis conformation is only observed in the atoms involved in a double bond.

Similarity in Solvent Structure between PITPα and PITPβ. The solvent structure within the lipid binding cavity was examined. The human PITPα structure complexed with phosphatidylinositol was determined to 2.95 Å, and no solvent structure was reported. A comparison of the interior solvent structure of the rat PITP-PtdCho isoforms indicates a high level of solvent structure conservation (Table 5 and Figure 4**)**. In rat PITPα-PtdCho 16 of the 18 (89%) lipid binding cavity solvent molecules are conserved in comparison to PITPβ-PtdCho, while 16 of the 20 (80%) internal water molecules of PITPβ-PtdCho are conserved relative to PITPα-PtdCho. The conservation of solvent structure extends not only to solvent molecules interacting directly with the phospholipid but also to water molecules in a second and third solvation shell around the ligand. A comparison to the mouse apo PITPα structure revealed that several of the conserved waters of the lipid-bound form of the protein are missing. In the apo PITPα structure, two water molecules (42 and 35) are located at the position of the phosphoryl oxygen atoms of the holo form of the proteins. Another solvent structure change near the phosphoryl group involves a rotamer change in Thr97, which is an absolutely conserved amino acid among all known PITP sequences. In the holo conformation of both PITP isoforms the Thr97 Oγ1 atom forms a hydrogen bond with a phosphoryl oxygen of the lipid. In contrast, this same side chain is rotated and forms a hydrogen bond with HOH180 in the apo PITPα conformation. Two solvent molecules in the apo form, HOH39 and HOH182, are situated close (within 1.45 Å) to the methyl groups of the choline moiety in the holo form.

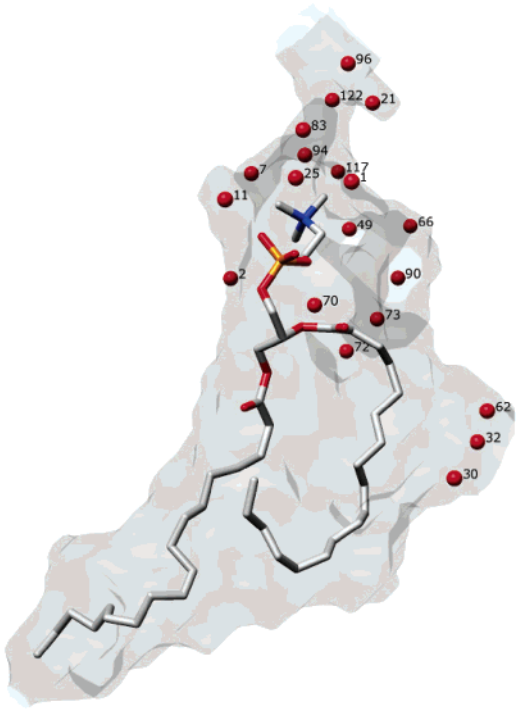

FIGURE 4: Solvent structure in lipid binding cavity. The lipid binding cavity of PITPβ-PtdCho is depicted as a gray isosurface. PtdCho is shown in sticks, with water molecules as red spheres.

Other water molecules in the apo form are displaced when PtdCho resides in the lipid binding cavity. In the apo conformation, HOH53 hydrogen bonds to the Glu218 Oϵ1 atom. In the holo conformation, Glu218 hydrogen bonds with the O11 atom of the *sn*-1 acyl ester linkage of PtdCho. There is no change in the rotamer conformation of Glu218 in the apo or holo form of the protein. HOH152 hydrogen bonds to the Glu86 Oϵ2 atom of apo PITPα; this water is displaced by the side chain of Glu86 in holo PITPα because β-strand 3 extends more into the cavity. Likewise, HOH198 and HOH216 from the apo PITPα structure are displaced by β-strands 2 and 3 that extend into their positions in the lipid-bound form of the protein.

Phospholipid Transfer Activities of Wild-Type Human and Rat PITP Isoforms. A comparison of human and rat PITP isoforms with respect to the intermembrane transfer of PtdIns, PtdCho, or Cer*P*Cho is shown in Table 6. A variety of membrane compositions were employed to highlight different aspects of protein-mediated lipid transfer. Using vesicles composed of PtdCho as the bulk lipid and PtdIns as a minor component (5 mol %), human PITPα, human PITPβ, and rat PITPα exhibited considerably higher rates for the transfer of PtdCho than for the transfer of PtdIns, even after normalizing to equivalent amounts of protein. In contrast, rat PITPβ was much less active toward PtdCho, a difference that led to nearly identical specific activities of PtdCho and PtdIns transfer. Employing vesicles in which PtdCho was the bulk lipid and Cer*P*Cho was present at 10 mol %, intermembrane sphingophospholipid flux mediated by the two mammalian PITPβ isoforms was comparable and higher than that mediated by the α isoforms.

With vesicles composed of PtdEtn as the bulk lipid and containing equal proportions of three transferable lipids (10 mol % each), a direct comparison among these lipids became possible. PtdIns clearly emerged as the preferred lipid substrate, followed by PtdCho at rates approximately 15−40% of those for PtdIns after normalizing to equivalent amounts of protein. Cer*P*Cho was a weak, yet reproducibly observed substrate. For the two radically different vesicle compositions, rates of PtdIns transfer were remarkably similar, within each group, for human PITPα, human PITPβ, and rat PITPα. Deviating from this trend was rat PITPβ, whose activity toward PtdIns and PtdCho was 30−60% of those of the other isoforms.

Phospholipid Transfer Specific Activities of Mutant Rat PITP Isoforms. Examination of the primary and tertiary structures of the lipid binding domains of rat PITPα and rat PITPβ led to the identification of amino acids that lay within 3.9 Å of the bound PtdCho but differed significantly in their chemistry (Figure 5). Two pairs of hydrophobic amino acids fulfilled these criteria: I84α/F83β and F225α/L224β. (These residues are superimposable but have different residue numbers due to the insertion of a single amino acid in PITPα after residue 51.) We hypothesized that these residues would account for some, if not all, of the observed differences in substrate specificity between the rat isoforms. Proteins were engineered to contain one or two point mutations in an effort to convert the PITPα phenotype to a PITPβ-like phenotype, and vice versa. Specific activities for the transfer of PtdIns, PtdCho, and Cer*P*Cho were then measured (Table 7).

As mutations were introduced into rat PITPα, there was little or no change in the transfer of PtdIns. In contrast, the F225αL mutation alone dramatically reduced the transfer of PtdCho and enhanced the transfer of Cer*P*Cho. The I84αF mutation appeared to play a minor role in altering substrate specificity. Complementary results were generally noted for comparable mutations introduced into rat PITPβ. The L224βF mutation affected all three lipid substrates, increasing the transfer of PtdIns and PtdCho and decreasing that of Cer*P*Cho. As we had observed with PITPα, the homologous F83βI mutation in PITPβ had little effect on the parent protein's lipid transfer activities. The activity of PITPβ (L224F) toward both glycerophospholipids was similar to

Table 6: Phospholipid Transfer Activities of Wild-Type Human and Rat Isoforms

vesicle lipid composition		lipid transfer substrate	transfer activity[a] (pmol·min^{-1}·ng^{-1})			
donors	acceptors		human PITPα	human PITPβ	rat PITPα	rat PITPβ
PtdCho/PtdIns/ LacPtdEtn (85:5:10 mol %)	PtdCho/PtdIns (95:5 mol %)	PtdIns	9.8 ± 0.9	10.2 ± 3.1	7.4 ± 1.1	4.3 ± 0.7
		PtdCho	19.0 ± 2.7	14.2 ± 1.5	22.3 ± 1.4	4.4 ± 0.3
PtdCho/Cer*P*Cho/ PtdOH/LacPtdEtn (78:10:2:10 mol %)	PtdCho/PtdOH (98:2 mol %)	Cer*P*Cho	0.04 ± 0.01	0.24 ± 0.01	0.05 ± 0.01	0.30 ± 0.01
PtdEtn/PtdIns/PtdCho/Cer*P*Cho/LacPtdEtn (60:10:10:10:10 mol %)	PtdCho/PtdOH (98:2 mol %)	PtdIns	6.2 ± 0.3	7.7 ± 1.1	9.8 ± 0.7	2.9 ± 0.4
		PtdCho	2.7 ± 0.1	1.9 ± 0.1	3.6 ± 0.4	0.4 ± 0.0
		Cer*P*Cho	0.04 ± 0.02	0.32 ± 0.01	0.13 ± 0.01	0.22 ± 0.01

[a] Results represent the mean ± SD of three to six measurements.

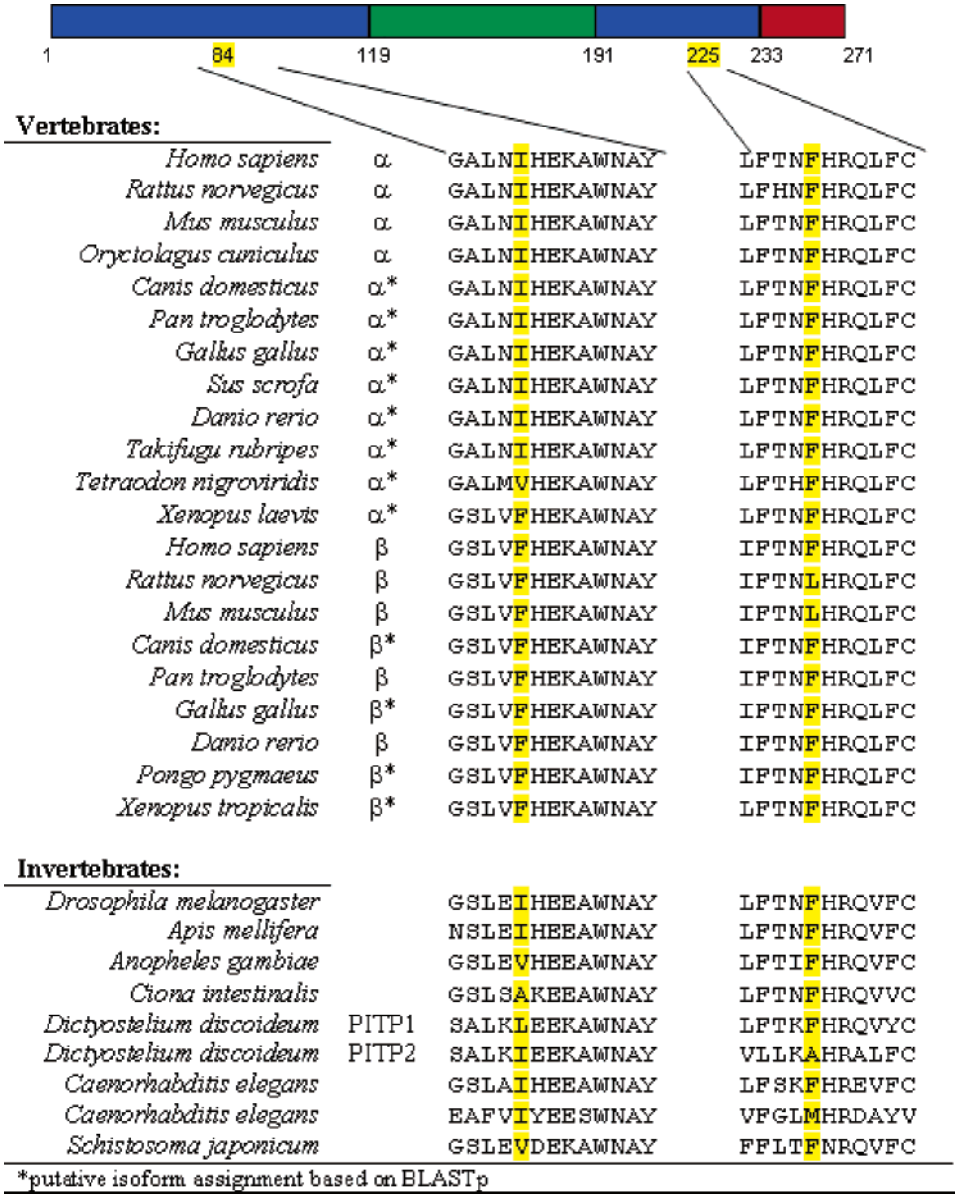

FIGURE 5: Species conservation of primary structure in the region of residues 84 and 225. Sequences surrounding the two sites of interest (yellow) in soluble PITPs from the indicated species are shown; residue 84 is in β-strand 4 and residue 225 is in α-helix F. Residue numbering is for rat PITPα. The cartoon depicts the three functional regions of PITP: lipid binding core (blue), regulatory loop (green), and C-terminal region (red). Isoform assignments for vertebrates are indicated following the species; an asterisk designates a putative assignment based on BLASTp alignment. Except for *D. discoideum* (*47*), invertebrate PITPs do not have a rigorous nomenclature for isoforms.

that of wild-type PITPα. Conversely, the activity of PITPα (F225L) toward PtdCho was, in fact, less than that of wild-type PITPβ. The incorporation of the second mutation, yielding PITPα (I84F/F225L) and PITPβ (F83I/L224F), led to a somewhat muted response compared to the singly mutated proteins, PITPα (F225L) and PITPβ (L224F). Mutations at the rat 225α/224β locus resulted in a partial conversion to the other isoform phenotype in regard to Cer*P*Cho transfer. In both isoforms, the double mutation did not amplify the effect of the single mutation in the 223/225 residue, although in the α isoform the PtdCho transfer specific activity was intermediate of the single mutations in each site.

DISCUSSION

The structure determination of rat PITPβ-PtdCho and the mutagenetic studies of the human and rat PITP isoforms were undertaken to explore differences in the lipid binding cavity and phospholipid substrate preferences. The primary conclusions from these studies are that the protein structures have high similarity with tight superposition, the phospholipid conformation exhibits subtle changes in acyl orientation, there is remarkable conservation of solvent structure around the lipid headgroup, and the mutation of two residues with differing physiochemical properties partially accounts for transfer rate differences between the two isoforms.

In comparing the lipid binding cavity in human and rat PITPs, it is apparent that flexibility of phospholipid ligands is tolerated. Some of this appears due to accommodation of different amino acid side chains, as seen for the *sn*-1 acyl chain in the rat structures at Ile84 in PITPα and at the corresponding Phe83 in PITPβ. The different orientation of the *sn*-1 and *sn*-2 acyl chains about the θ_3/θ_4 torsion angle of the glycerol backbone in the PtdIns-bound and the PtdCho-

Table 7: Phospholipid Transfer Activity of Rat Wild-Type and Mutant PITPs

protein species	transfer activity[a] (pmol·min^{-1}·ng^{-1})		
	PtdIns[b]	PtdCho[c]	Cer*P*Cho[d]
PITPα	6.1 ± 1.3	10.9 ± 0.4	0.05 ± 0.01
PITPα (I84F)	5.3 ± 0.6	11.2 ± 1.7	0.03 ± 0.01
PITPα (F225L)	5.5 ± 1.2	4.4 ± 0.6	0.10 ± 0.00
PITPα (I84F,F225L)	6.4 ± 0.4	7.4 ± 1.0	0.10 ± 0.00
PITPβ	3.3 ± 0.2	6.4 ± 0.2	0.30 ± 0.01
PITPβ (F83I)	3.3 ± 0.9	5.6 ± 0.9	0.29 ± 0.04
PITPβ (L224F)	6.2 ± 0.7	9.5 ± 1.1	0.20 ± 0.01
PITPβ (F83I,L224F)	6.6 ± 0.3	8.3 ± 1.4	0.19 ± 0.01

[a] Amount of protein assayed is 5−150 ng (0.15−4.7 pmol); results represent the mean ± SD of three measurements. [b] Donor vesicles contained PtdCho/PtdIns/LacPtdEtn (80:10:10 mol %); acceptor vesicles contained PtdCho/PtdOH (98:2 mol %). [c] Donor vesicles contained PtdCho/PtdOH/LacPtdEtn (88:2:10 mol %); acceptor vesicles contained PtdCho/PtdOH (98:2 mol %). [d] Donor vesicles contained PtdCho/Cer*P*Cho/PtdOH/LacPtdEtn (78:10:2:10 mol %); acceptor vesicles contained PtdCho/PtdOH (98:2 mol %).

bound forms of PITPα and PITPβ of the isoforms may be due to lack of a preferred orientation about the carbon 1 and 2 atoms of the glycerol backbone, differences in the acyl chain composition of the two structures, or ambiguity arising from the difference in resolution in the experimental data of the two structures.

In all PITP structures, 34.6% of the acyl chain torsion angles are trans (ap), while 36.9% are skew (±ac). All cis bonds are accounted for by the double bonds observed in the PtdCho structures. The headgroup conformations in all three structures share the most similar conformation and are not found in the typical "bent-down" conformation observed in phospholipid crystal structures. There are extensive interactions with protein side chains and with solvent molecules. Marsh (*40*) argues that the prevalence of skew conformations in protein-bound phospholipids is likely indicative of conformational heterogeneity of the lipids. The electron density of the acyl chains is somewhat indistinct when compared to density for the protein which has carbonyl bulges and −R groups that provide conformational landmarks for model building. Nevertheless, the acyl chains in the PITPs with chemically homogeneous phospholipids do not show significant conformational heterogeneity that would manifest itself in weak electron density.

In comparing the transfer activity of the human and rat PITP isoforms, it is clear that the β isoforms have the least differences in the transfer rate preference between PtdIns and PtdCho when donor receptors contain predominantly PtdCho. When PtdCho and PtdIns are present in equivalent concentrations in donor vesicles, PtdIns transfer occurs at approximately 3-fold the rate of PtdCho. The rat PITPβ isoform clearly has the most diminished transfer rate of the four proteins studied here. Due to the high sequence conservation between these proteins, there are limited residues that differ in all three proteins and are the subject of continued investigation. It is clear that many factors affect phospholipid transfer, both in vivo and in vitro. Phospholipid exchange was analyzed under controlled, in vitro conditions in this study. The effect of the mutations in this study may be different under more physiological conditions, and further study is warranted. A possible discriminating factor may be acyl chain length of the phospholipids. PITPα has been shown to have a preference for shorter acyl chains in both PtdIns and PtdCho (*41*). Nevertheless, usage of carefully controlled vesicle phospholipid composition in this study allows direct comparison of vesicles of known composition.

Of the two amino acid loci in mammalian PITPs that were investigated in the current study, 225α/224β proved to be the more critical in determining substrate specificity. This locus is a Phe in all vertebrates of known sequence except for the rat and mouse, which both possess a Leu in PITPβ. When the large, aromatic Phe residue occupies this locus, the intermembrane transfer of PtdCho is high. On the other hand, when the smaller, aliphatic Leu residue occupies this position, PtdCho transfer is lower by a factor of about 2. This is the only single site polymorphism that we are aware of that decreases PtdCho transfer but does not affect PtdIns transfer. Following the in vitro mutation of this locus to the other amino acid, the PtdCho transfer specific activity became nearly identical to that of the other wild-type isomer, i.e., rat PITPα (F225L) $\approx$ PITPβ and rat PITPβ (L224F) $\approx$ PITPα (Table 7). Confirming the role of this locus in influencing the transfer activity toward PtdCho, the two human PITP isoforms and rat PITPα, all of which contain Phe at the locus, have comparable activities toward PtdCho (Table 6). More significantly, their activities were well above that of rat PITPβ.

For the other glycerophospholipid substrate PtdIns, mutations at the 225α/224β locus do not exhibit such clear-cut effects on phospholipid transfer specificity. While rat PITPβ (L224F) exhibited activity indistinguishable from that of PITPα with respect to PtdIns transfer, rat PITPα (F225L) retained its parental phenotype (Table 7). The two human PITP isoforms, which contain the same residue as their rat counterparts at this position, have equivalent PtdIns transfer activity, and it is comparable to the rat PITPα isoform. Furthermore, only the rodents do not maintain the strict conservation of a Phe at this location when comparing vertebrate sequences at this position (Figure 5).

The 225α/224β locus, in contrast, played a much more modest role in the specificity of both isoforms toward Cer*P*Cho. When the small, aliphatic residue Leu occupies this locus in either rat PITP isoform, the transfer of Cer*P*Cho is elevated; conversely, when Phe occupies this position, the transfer of Cer*P*Cho is diminished. It is surprising, however, that both human PITP isoforms contain a Phe at this locus and their relative activity to PtdIns is similar to rat PITPα while their activities toward PtdCho are similar to their respective rat homologues. The transfer rates of Cer*P*Cho are significantly lower than the transfer of either PtdIns or PtdCho for any of the PITP isoforms studied. Although PITPβ clearly transports Cer*P*Cho more effectively than the α isoform in the in vitro assay system used, the physiological role of transfer of this lipid has not been resolved. Sphingolipids represent a small class of lipids in eukaryotic membranes but have been shown to be important in cell development, signal transduction, and protein sorting (*42*). Complicating the issue is the localization of the majority of the membrane Cer*P*Cho on the exoplasmic surface (*43*) and a corresponding small pool that is accessible to cytosolic PITPs. Cer*P*Cho and cholesterol are often found in microdomains known as rafts and caveloae, which effectively localize concentration levels, up to 50% or more (*44*, *45*). PITPβ, but not PITPα, has been shown to facilitate Cer*P*Cho

transport in vesicles with greater than 0.4 mol % cholesterol. This level of cholesterol leads to liquid-crystalline complexes with the coexistence of liquid-disordered and liquid-ordered phases, perhaps mimicking membrane rafts and caveloae (*27*).

Clearly, a complete explanation of the differences in phospholipid transfer activity cannot be explained by these two loci alone. The role of these residues during phospholipid exchange, which requires considerable conformational changes within the protein, is unknown. The PITP lipid binding cavity is large and accommodates structurally diverse substrates, possibly allowing compensatory changes to offset mutations within individual binding sites. Nevertheless, residues lining the lipid binding cavity are highly conserved, including a number of aromatic residues. These aromatic residues have the potential to form cation$-\pi$ bonds with the ligand during the exchange process, perhaps playing a role in the transfer rate even though they appear somewhat distant in the statically bound protein state. Additional biophysical techniques will be necessary to elucidate the role of these, and other, residues during phospholipid transfer.

ACKNOWLEDGMENT

Data were collected at Southeast Regional Collaborative Access Team (SER-CAT) 22-ID beamline at the Advanced Photon Source, Argonne National Laboratory. We gratefully acknowledge the assistance of Stephen Foundling with X-ray data collection. Supporting institutions may be found at www.ser-cat.org/members.html. Use of the Advanced Photon Source was supported by the U.S. Department of Energy, Office of Science, Office of Basic Energy Sciences, under Contract No. W-31-109-Eng-38.

REFERENCES

1. Routt, S. M., and Bankaitis, V. A. (2004) Biological functions of phosphatidylinositol transfer proteins, *Biochem. Cell Biol. 82*, 254−262.
2. Allen-Baume, V., Segui, B., and Cockcroft, S. (2002) Current thoughts on the phosphatidylinositol transfer protein family, *FEBS Lett. 531*, 74−80.
3. van Tiel, C. M., Schouten, A., Snoek, G. T., Gros, P., and Wirtz, K. W. A. (2002) The structure of phosphatidylinositol transfer protein α reveals sites for phospholipid binding and membrane association with major implications for its function, *FEBS Lett. 531*, 69−73.
4. Hay, J. C., and Martin, T. F. J. (1993) Phosphatidylinositol transfer protein is required for ATP-dependent priming of Ca^{2+}-activated secretion, *Nature 366*, 572−575.
5. Ohashi, M., de Vries, K. J., Frank, R., Snoek, G., Bankaitis, V., Wirtz, K., and Huttner, W. B. (1995) A role for phosphatidylinositol transfer protein in secretory vesicle formation, *Nature 377*, 544−547.
6. Cunningham, E., Tan, S. K., Swigart, P., Hsuan, J., Bankaitis, V., and Cockcroft, S. (1996) The yeast and mammalian isoforms of phosphatidylinositol transfer protein can all restore phospholipase C-mediated inositol lipid signaling in cytosol-depleted RBL-2H3 and HL-60 cells, *Proc. Natl. Acad. Sci. U.S.A. 93*, 6589−6593.
7. Jones, S. M., Alb, J. G. J., Phillips, S. E., Bankaitis, V. A., and Howell, K. E. (1998) A phosphatidylinositol 3-kinase and phosphatidylinositol transfer protein act synergistically in formation of constitutive transport vesicles from the trans-Golgi network, *J. Biol. Chem. 273*, 10349−10354.
8. Dickeson, S. K., Helmkamp, G. M., Jr., and Yarbrough, L. R. (1994) Sequence of a human cDNA encoding phosphatidylinositol transfer protein and occurrence of a related sequence in widely divergent eukaryotes, *Gene 142*, 301−305.
9. Yoder, M. D., Thomas, L. M., Tremblay, J. M., Oliver, R. L., Yarbrough, L. R., and Helmkamp, G. M., Jr. (2001) Structure of a multifunctional protein: mammalian phosphatidylinositol transfer protein complexed with phosphatidylcholine, *J. Biol. Chem. 276*, 9246−9252.
10. Schouten, A., Agianian, B., Westerman, J., Kroon, J., Wirtz, K. W. A., and Gros, P. (2002) Structure of apo-phosphatidylinositol transfer protein α provides insight into membrane association, *EMBO J. 21*, 2117−2121.
11. Tilley, S. J., Skippen, A., Murray-Rust, J., Swigart, P. M., Stewart, A., Morgan, C. P., Cockcroft, S., and McDonald, N. Q. (2004) Structure−function analysis of phosphatidylinositol transfer protein alpha bound to human phosphatidylinositol, *Structure 12*, 317−326.
12. Sha, B., Phillips, S. E., Bankaitis, V. A., and Luo, M. (1998) Crystal structure of the *Saccharomyces cerevisiae* phosphatidylinosito transfer protein, *Nature 391*, 506−510.
13. Roderick, S. L., Chan, W. W., Agate, D. S., Olsen, L. R., Vetting, M. W., Rajashankar, K. R., and Cohen, D. E. (2002) Structure of human phosphatidylcholine transfer protein in complex with its ligand, *Nat. Struct. Biol. 9*, 507−511.
14. Romanowski, M. J., Soccio, R. E., Breslow, J. L., and Burley, S. K. (2002) Crystal structure of the *Mus musculus* cholesterol-regulated START protein 4 (StarD4) containing a StAR-related lipid transfer domain, *Proc. Natl. Acad. Sci. U.S.A. 99*, 6949−6954.
15. de Vries, K. J., Heinrichs, A. A., Cunningham, E., Brunink, F., Westerman, J., Somerharju, P. J., Cockcroft, S., Wirtz, K. W. A., and Snoek, G. T. (1995) An isoform of the phosphatidylinositol-transfer protein transfers sphingomyelin and is associated with the Golgi system, *Biochem. J. 310*, 643−649.
16. de Vries, K. J., Westerman, J., Bastiaens, P. I., Jovin, T. M., Wirtz, K. W. A., and Snoek, G. T. (1996) Fluorescently labeled phosphatidylinositol transfer protein isoforms (α and β), microinjected into fetal bovine heart endothelial cells, are targeted to distinct intracellular sites, *Exp. Cell Res. 277*, 33−39.
17. van Tiel, C. M., Westerman, J., Paasman, M. A., Hoebens, M. M., Wirtz, K. W. A., and Snoek, G. T. (2002) The Golgi localization of phosphatidylinositiol transfer protein β requires the protein kinase C-dependent phosphorylation of serine 262 and is essential for maintaining plasma membrane sphingomyelin levels, *J. Biol. Chem. 277*, 22447−22452.
18. Snoek, G. T., Berrie, C. P., Geijtenbeek, T. B. H., van der Helm, H. A., Cadee, J. A., Lurisci, C., Corda, D., and Wirtz, K. W. A. (1999) Overexpression of phosphatidylinositol transfer protein α in NIH3T3 cells activates a phospholipase A, *J. Biol. Chem. 274*, 35393−35399.
19. van Tiel, C. M., Luberto, C., Snoek, G. T., Hannun, Y. A., Wirtz, K. W. A. (2000) Rapid replenishment of sphingomyelin in the plasma membrane upon degradation by sphingomyelinase in NIH3T3 cells overexpressing the phosphatidylinositol transfer protein β, *Biochem J. 346*, 537−543.
20. Bankaitis, V. A. (2002) Slick recruitment to the Golgi, *Science 295*.
21. Hamilton, B. A., Smith, D. J., Mueller, K. L., Kerrebrock, A. W., Bronson, R. T., van Berkel, V., Daly, M. J., Kruglyak, L., Reeve, M. P., Nemhauser, J. L., Hawkins, T. L., Rubin, E. M., and Lander, E. S. (1997) The *vibrator* mutation causes neurodegeneration via reduced expression of PITPα: positional complementation cloning and extragenic suppression, *Neuron 18*, 711−722.
22. Alb, J. G. J., Cortese, J. D., Phillips, S. E., Albin, R. L., Nagy, T. R., Hamilton, B. A., and Bankaitis, V. A. (2003) Mice lacking phosphatidylinositol transfer protein-α exhibit spinocerebellar degeneration, intestinal and hepatic steatosis, and hypoglycemia, *J. Biol. Chem. 278*, 33501−33518.
23. Dickeson, S. K., Lim, C. N., Schuyler, G. T., Dalton, T. P., Helmkamp, G. M. J., and Yarbrough, L. R. (1989) Isolation and sequence of cDNA clones encoding rat phosphatidyl:inositol transfer protein, *J. Biol. Chem. 264*, 16557−16564.
24. Cawley, D. B., Hedblom, M. L., and Houston, L. L. (1978) Homology between ricin and *Ricinus communis* agglutinin: amino terminal sequence analysis and protein synthesis inhibition studies, *Arch. Biochem. Biophys. 190*, 744−755.
25. Tremblay, J. M., Helmkamp, G. M., Jr., and Yarbrough, L. R. (1996) Limited proteolysis of rat phosphatidylinositol transfer protein by trypsin cleaves the C terminus, enhances binding to lipid vesicles, and reduces phospholipid transfer activity, *J. Biol. Chem. 271*, 21075−21080.
26. Voziyan, P. A., Tremblay, J. M., Yarbrough, L. R., and Helmkamp, G. M., Jr. (1996) Truncations of the C-terminus have different

effects on the conformation and activity of phosphatidylinositol transfer proteins, *Biochemistry 35*, 12526−12531.
27. Miller, E. C., and Helmkamp, G. M. J. (2003) Exposure of phosphatidylinositol transfer proteins to sphingomyelin-cholesterol membranes suggests transient but productive interactions with raft-like, liquid-ordered domains, *Biochemistry 42*, 13250−13259.
28. Kasper, A. M., and Helmkamp, G. M., Jr. (1981) Protein-catalyzed phospholipid exchange between gel and liquid-crystalline phospholipid vesicles, *Biochemistry 20*, 146−151.
29. Oliver, R. L., Tremblay, J. M., Helmkkamp, G. M., Jr., Yarbrough, L. R., Breakfield, N. W., and Yoder, M. D. (1998) X-ray analysis of crystals of rat phosphatidylinositol transfer protein with bound phosphatidylcholine, *Acta Crystallogr. D55*, 522−524.
30. Otwinowski, Z., and Minor, W. (1997) Processing of X-ray diffraction data collected in oscillation mode, *Methods Enzymol. 276*, 307−326.
31. Collaborative Computer Project Number 4 (1994) The CCP4 suite: programs for protein crystallography, *Acta Crystallogr. D50*, 760−763.
32. Jones, T. A., Zou, J.-Y., Cowan, S. W., and Kjeldgaard, M. (1991) Improved methods for the building of protein models in electron density maps and the location of errors in these models, *Acta Crystallogr. A47*, 110−119.
33. Brunger, A. T., Adams, P. D., Clore, G. M., Delano, W. L., Gros, P., Grosse-Kunstleve, R. W., Jiang, J.-S., Kuszewski, J., Nilges, M., Pannu, N. S., Read, R. J., Rice, L. M., Simonson, T., and Warren, G. L. (1998) Crystallography & NMR system: A new software suite for macromolecular structure determination, *Acta Crystallogr. D54*, 905−921.
34. Brünger, A. T. (1993) Assessment of phase accuracy by cross validation: the free *R* value. Methods and applications, *Acta Crystallogr. D49*, 24−36.
35. Lawkowski, R. A., MacArthur, M. W., Moss, D. S., and Thornton, J. M. (1992) PROCHECK: a program to check the stereochemical quality of protein structures, *J. Appl. Crystallogr. 26*, 283−291.
36. Nicholls, A., Sharp, K., and Honig, B. (1991) Protein folding and association: insights from the interfacial and thermodynamic properties of hydrocarbons, *Proteins 11*, 281−296.
37. Guex, N., and Peitsch, M. C. (1997) SWISS-MODEL and the Swiss-PdbViewer: An environment for comparative protein modeling, *Electrophoresis 18*, 2714−2723.
38. Kleywegt, G. J., and Jones, T. A. (1994) Detection, delineation, measurement and display of cavities in macromolecular structures, *Acta Crystallogr. D50*, 178−185.
39. Schrauber, H., Eisenhaber, F., and Argos, P. (1993) Rotamers: To be or not to be? An analysis of amino acid side-chain conformations in globular proteins, *J. Mol. Biol. 230*, 592−612.
40. Marsh, D. (2003) Lipid-binding proteins: Structure of the phospholipid ligands, *Protein Sci. 12*, 2109−2117.
41. Hunt, A. N., Skippen, A. J., Koster, G., Postle, A. D., and Cockcroft, S. (2004) Acyl chain-based molecular selectivity for HL60 cellular phosphatidylinositol and of phosphatidylcholine by phosphatidylinositol transfer protein α, *Biochim. Biophys. Acta 1686*, 50−60.
42. Slimane, T. A., and Hoekstra, D. (2002) Sphingolipid trafficking and protein sorting in epithelial cells, *FEBS Lett*.
43. Zhang, P., Liu, B., Jenkins, G. M., Hannun, Y. A., and Obeid, L. M. (1997) Expression of neutral sphingomyelinase identifies a distinct pool of sphingomyelin involved in apoptosis, *J. Biol. Chem. 272*, 9609−9612.
44. Lange, Y., Swaisgood, M. H., Ramos, R. V., and Steck, T. L. (1989) Plasma membranes contain half the phospholipid and 90% of the cholesterol and sphingomyelin in cultured human fibroblasts, *J. Biol. Chem. 264*, 3786−3793.
45. Pike, L. J. (2003) Lipid rafts: bringing order to chaos, *J. Lipid Res. 44*, 655−667.
46. Hauser, H., Pascher, I., Pearson, R. H., and Sundell, S. (1981) Preferred conformation and molecular packing of phosphatidylethanolamine and phosphatidylcholine, *Biochim. Biophys. Acta 650*, 21−51.
47. Swigart, P., Insall, R., Wilkins, A., and Cockcroft, S. (2000) Purification and cloning of phosphatidylinositol transfer proteins from *Dictyostelium discoideum*: homologues of both mammalian PITPs and *Saccharomyces cerevisiae* Sec14p are found in the same cell, *Biochem. J. 347*, 837−843.

BI051191R